Brain Surface Analysis for Dementia Diagnosis

A. Alansary [1,*], M. Nitzken[1,*], A. Black, A. Elnakib[1], F. Khalifa[1], k. Katti, A. Soliman[1], M. Mostapha[1], M. F. Casanova[2], and A. El-Baz[1,**]

[1]BioImaging Laboratory, Bioengineering Department, University of Louisville, Louisville, KY, USA.
[2]Department of Psychiatry and Behavioral Science, University of Louisville, Louisville, KY, USA.

Abstract. A comprehensive framework for the early diagnosis of dementia diseases using T1-weighted magmatic resonance imaging (MRI) of the brain is proposed. The analysis framework consists of two main stages: brain extraction and shape analysis and diagnosis. First, the brain tissue (i.e., white matter, gray matter) is extracted by following a procedure like most conventional approaches. Namely, the T1-weighted MR brain images and desired maps of regions (brain and non-brain) are modeled by a joint Markov-Gibbs random field (MGRF) model of independent image signals and interdependent region labels. The proposed joint MGRF model accounts for the following three descriptors: *i*) a first-order visual appearance descriptor that closely approximate the empirical distribution of signal intensity using sign alternate Gaussian models, *ii*) a 3D probabilistic shape prior that is learned using a subset of 3D co-aligned training T1-weighted MR brain images, and *iii*) a 3D spatially invariant homogeneity descriptor that is modeled by a second-order translation and rotation invariant MGRF of 3D T1-weighted MR brain region labels with analytically estimated potentials. Secondly, a shape analysis step is performed by extracting different brain features that are derived from the variability of the extracted brain using a spherical harmonic (SPHARM) analysis. We describe the brain shape complexity with two new shape indexes, the error in SPHARM reconstruction and the surface complexity. Then, a K-nearest neighbor classifier is used to discriminate between Alzheimer's disease (AD) mild cognitive impairment (MCI), and controls subjects.

Keywords: Dementia, Alzheimer's disease, 3D Probabilistic Shape, MGRF

1   Introduction

Dementia brain diseases (e.g., Alzheimer, vascular dementia) are among the most interesting and challenging research areas in modern neuroscience. Alzheimer's disease (AD) is the most common cause of a progressive dementia that accounts for 60-80% percent of cases [1]. The AD is characterized by the decline in mental

---

* Equal Contribution
** Corresponding author:- Tel:(502)-852-5092, E-mail: aselba01@louisville.edu

ability which severely affects the thinking and social abilities interfere of the adults in the daily life [1]. Therefore, early diagnosis of dementia diseases is of great important to institute appropriate therapies. In this paper, we propose a a computer-aided diagnostic (CAD) system of dementia using structural T1-Weighted MRI data of the brain. Instead of examining the volumetric changes in individual brain structures, the proposed CAD system attempts to analyze and quantify differences between the whole 3D brain shapes for AD, mild cognitive impairment (MCI), and controls subjects in order to discriminate between them more accurately.

Developing CAD system for the clinical diagnosis of dementia diseases essentially requires accurate delineation of the brain tissue, i.e., white and grey matters [2]. Thus, the first step of our framework performs skull stripping and brain segmentation. The proposed brain segmentation is based on the integration of statistical approaches (a probabilistic shape prior, first-order intensity model, and second-order appearance model) that are integrated into a two-level joint Markov-Gibbs random field (MGRF) model of T1-MR brain images. Following brain segmentation, we generate a 3D mesh model of a manifold of the brain surface, and after mapping this to a unit sphere we approximate the original shape using spherical harmonic (SPHARM) analysis. We then use the SPHARM reconstruction error and surface complexity of the manifold as indexes to describe the overall complexity of the brain shape. These features are augmented into a k-nearest neighbor classifier to distinguish between Alzheimer's disease (AD) mild cognitive impairment (MCI), and controls subjects. Details of the proposed framework are described below.

2   Brain Segmentation using Joint MGRF Model

Let $\mathbf{Q} = \{0, \ldots, Q-1\}$ and $\mathbf{L} = \{1, \ldots, L\}$ denote sets of gray levels q and region labels L, respectively. Let $\mathbf{R}$ denote a 3D arithmetic (x, y, z)-lattice that supports a given grayscale image $\mathbf{g} : \mathbf{R} \to \mathbf{Q}$ to be segmented and its goal labled region map $\mathbf{m} : \mathbf{R} \to \mathbf{L}$. The 3D T1-weighted MR brain images, $\mathbf{g}$, being co-aligned to the 3D training data, and its map, $\mathbf{m}$, are described with the following joint probability model

$$P(\mathbf{g}, \mathbf{m}) = P(\mathbf{g}|\mathbf{m})P(\mathbf{m}) \tag{1}$$

that combines a 3D second-order Markov-Gibbs random field (MGRF), $P(\mathbf{m})$, of region labels with the shape prior of the brain and a conditionally independent random field. The joint conditional distribution of image intensities given the map is $P(\mathbf{g}|\mathbf{m}) = \prod_{(x,y,z) \in \mathbf{R}} p(g_{x,y,z}|m_{x,y,z})$. The map model $P(\mathbf{m}) = P_{\text{sp}}(\mathbf{m})P_{\text{h}}(\mathbf{m})$ has two parts: (*i*) a shape prior probability $P_{\text{sp}}(\mathbf{m})$, and (*ii*) a second-order MGRF model $P_{\text{h}}(\mathbf{m})$ of a spatially homogeneous region map $\mathbf{m}$ for the image $\mathbf{g}$, which is aligned to the training set. In this work we focus on accurate identification of the spatial interaction between the brain voxels ($P(\mathbf{m})$) and the 1st-order visual appearance descriptor for the brain tissues ($P(\mathbf{g}|\mathbf{m})$) as shown in Fig. 1.
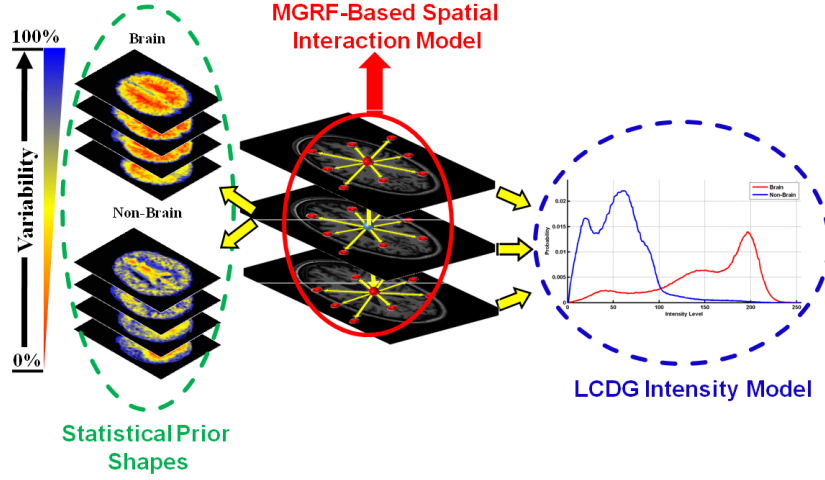
Fig. 1. Illustration of the proposed joint Markov-Gibbs model of T1-weighted MR brain images.

2.1 Shape Model

To enhance the segmentation accuracy, expected shapes of the brain is constrained with a probabilistic shape prior. To construct the shape prior, a training set of 3D MR brain images collected for different subjects are co-aligned by 3D affine transformations with 12 degrees of freedom in a way that maximizes their mutual information (MI) [3]. The shape prior is a spatially variant independent random field of region labels $P_{\text{sp}}(\mathbf{m}) = \prod_{(x,y,z) \in \text{R}} p_{\text{sp}:x,y,z}(m_{x,y,z})$ for the co-aligned, manually segmented data sets, specified by voxel-wise empirical probabilities for the brain and non-brain labels $(p_{\text{sp}:x,y,z}(l), l \in \mathbf{L}$.

For the training phase, we use 30 data sets that were first segmented using the FMRIB's automated segmentation tool [4] and then corrected manually by MR experts. Then, the segmented images are used to create the probabilistic map of the brain. During the testing phase, each data to be segmented is globally registered with the set of training data that have been used to create the prior shape model of the brain.

2.2 1st-Order Visual Appearance Descriptor

In addition to the learned prior shape descriptor, we implement a 1st-order visual appearance descriptor of the MR images. During segmentation of a data set, this visual appearance descriptor is roughly taken into account by approximating the 1D empirical marginal gray level distributions of the T1-weighted MR brain images with a linear combinations of discrete Gaussians (LCDG) [5–7]. This LCDG model is a modified version of our previous linear combination of

continuous Gaussian probabilistic model [8,9]. This approximation adapts the segmentation to the changing appearance, such as non-linear intensity variations caused by patient weight and data acquisition systems (e.g. scanner types and scanning parameters). The LCDG models the empirical distribution the brain (white matter and grey matter) and non-brain (CSF and other brain structures) tissues label more accurately than a conventional mixture of only positive Gaussians. This yields a better initial region map that is formed by the voxel-wise classification of the gray values in the images.

Let $\mathbf{F} = \left(f(q) : q \in \mathbf{Q}; \sum_{q \in \mathbf{Q}} f(q) = 1 \right)$ be an empirical marginal probability distribution of gray levels, q, for the 3D T1-weighted MR brain image, $\mathbf{g}$. Each distribution has a known number, L, of dominant modes related to the regions of interest (in our case, $L = 2$). To segment an image by separating these individual dominant modes, the individual gray level distributions that are associated with each mode must be estimated from $\mathbf{F}$. Unlike conventional modeling with a mixture of Gaussians [10], or another simple distribution type [11] where there is only one distribution per dominant mode, we approximate $\mathbf{F}_j$ much more closely using the LCDG. The LCDG is partitioned for the whole image into multiple LCDG submodels that each relate to a unique dominant mode (in our case brain and non-brain structures). The discrete Gaussian (DG) components $\Psi_\gamma = (\psi(q|\gamma) : q \in \mathbf{Q})$ then integrate a continuous Gaussian with parameters $\gamma = (\mu, \sigma^2)$; where μ and σ^2 are the mean and the variance, respectively, over successive gray level intervals. The LCDG with C_p positive and C_n negative components, such that $C_\mathrm{p} \geq L$, is defined as follows [5,8]:

$$P_{\mathbf{w},\Theta}(q) = \sum_{r=1}^{C_\mathrm{p}} w_{\mathrm{p},r}\psi(q|\gamma_{\mathrm{p},r}) - \sum_{t=1}^{C_\mathrm{n}} w_{\mathrm{n},t}\psi(q|\gamma_{\mathrm{n},t}) \qquad (2)$$

with the non-negative weights $\mathbf{w} = [w_{p,.}, w_{n,.}]$ such that $\sum_{r=1}^{C_\mathrm{p}} w_{\mathrm{p},r} - \sum_{t=1}^{C_\mathrm{n}} w_{\mathrm{n},t} = 1$. In order to precisely estimate the parameters of the LCDG model, including the numbers of positive and negative components, EM-based techniques, namely those introduced in [5] for approximation of a probability density model when using a linear combination of Gaussians, have been adapted to this LCDG model.

2.3   3D Spatial Interaction MGRF Model

In order to perform a more accurate segmentation, spatially homogeneous 3D pair-wise interactions between the region labels are additionally incorporated in the model. These interactions are calculated using popular Potts model (i.e., an MGRF with the nearest 26-neighbors of the voxels as demonstrated in Fig. 2), and analytic bi-valued Gibbs potentials, that depend only on whether the nearest pairs of labels are equal or not. Let $f_\mathrm{eq}(\mathbf{m})$ denote the relative frequency of equal labels in the neighboring voxel pairs $((x,y,z),(x+\xi,y+\eta,z+\zeta)) \in \mathbf{R}^2$; $(\xi,\eta,\zeta) \in (\pm1,0,0),(0,\pm1,0),(\pm1,\pm1,0),\pm1,0,\pm1),(0,\pm1,\pm1),(\pm1,\pm1,\pm1)$. The initial region map results in an approximation with the following analytical

maximum likelihood estimates of the potentials [5, 12]:

$$v_{\text{eq}} = -v_{\text{ne}} \approx 2f_{\text{eq}}(\mathbf{m}) - 1 \qquad (3)$$

that allow for computing the voxel-wise probabilities $p_{\text{h}:x,y,z}(m_{x,y,z} = l)$ of each label; $l \in \mathbf{L}$.

One of the advantages of the proposed approach is that it addresses the inhomogeneities in the transition regions of different brain structures. At these transition locations, there is typically a spatial inhomogeneity in the signal intensity [13]. Importantly, in addition to signal intensity, our approach uses shape and spatial interaction components. This provides additional information that aids in overcoming the variability that often results when solely taking signal intensities into account. The proposed step-wise segmentation algorithm is summarized in Algorithm 1 and Fig. 3.

Algorithm 1: Key Steps for the Proposed Segmentation Approach

---

1. Remove the skull from T1-weighted MR brain images using the approach proposed in [14].
2. Approximate the marginal intensity distribution $P(\mathbf{g})$ of the T1-weighted MR brain image using LCDG with four dominant modes.
3. Form an initial region map $\mathbf{m}$ using the marginal estimated density and prior shape of each brain label.
4. Find the Gibbs potentials for the MGRF model from the initial map by using Eq. 3.
5. Improve the region map $\mathbf{m}$ using voxel-wise Bayes classifier.
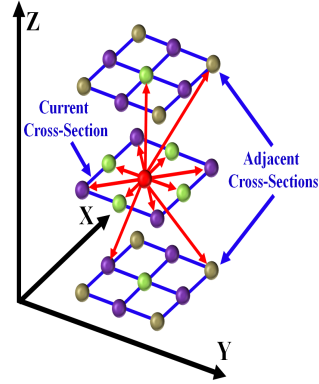
Fig. 2. Illustration of the proposed 3D neighborhood system.

3   Brain Shape Analysis and Dementia Diagnosis

Following brain segmentation, a 3D mesh model of the brain surface is mapped to a unit sphere, and approximated with a linear combination of spherical Hharmonics (SPHARM). The number of SPHARMs used in reconstruction yields a desired approximation accuracy that can be used as a new shape index to describe the complexity of the brain shape. Then, a K-nearest classifier separates the AD, MCI, and controls subjects by their shape indexes.

Spectral SPHARM analysis [15, 16] considers a set of 3D surface data as a linear combination of specific basis functions. We perform a weighted-SPHARM analysis similar to the approach that was used in our previous work on autism [17]. The surface manifold of the brain is approximated using a Delaunay triangulated 3D mesh (see Fig. 4), having 50,000 nodes, constructed using an algorithm based on the work of Fang and Boas [18]. Secondly, the brain mesh for each
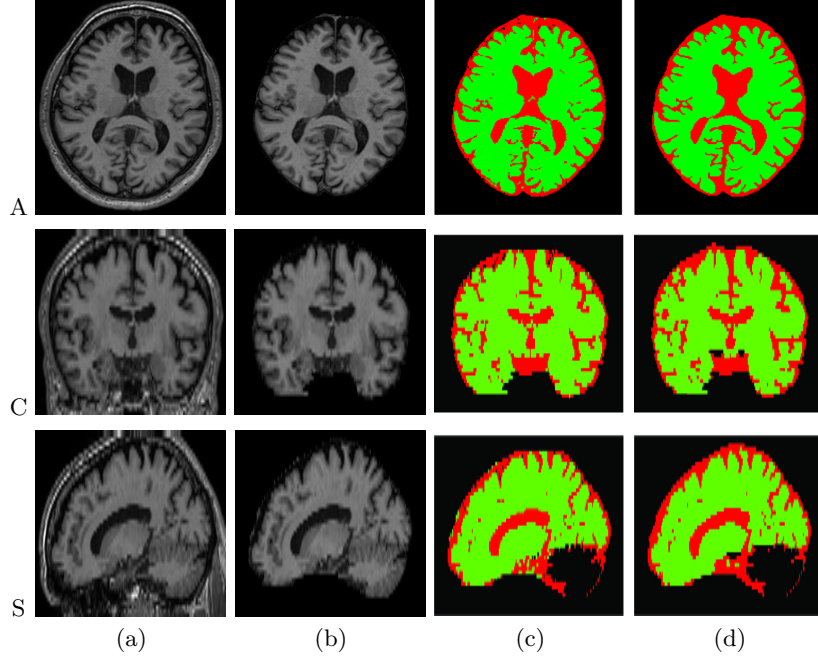
Fig. 3. Segmentation results of the proposed segmentation approach. Segmentation performed in 3D; results projected onto 2D axial (A), coronal (C), and sagittal (S) planes for visualization. (a) 2D profile of the original T1-weighted MR brain images, (b) MR brain data after removing the skull [14], (c) initial segmentation results using 1st-order visual appearance and prior shape models, and (d) final segmentation results using the proposed three models. Note that the brain (white and grey matters) and non-brain tissues are shown green, and red colors, respectively.

subject is mapped to a unit sphere utilizing a novel mapping approach [17], called "*Attraction-Repulsion*" that calls for all the mesh nodes to meet two conditions: (*i*) the unit distance of each node from the brain center, and (*ii*) an equal distance of each node from all of its nearest neighbors.

The brain mesh is then approximated using a linear combination of spherical harmonics. In general, the theory is that lower-order harmonics are sufficient to represent the more generic shape information of the brain. The higher-order harmonics contain the fine details of the brain and help to rebuild the nuanced gyrifications of the brain shape. A SPHARM analysis is performed by solving an isotropic heat equation for the brain surface on the unit sphere [16, 17].

Let $\mathcal{S} : \mathbf{M} \to \mathbf{U}$ denote the mapping of a brain mesh $\mathbf{M}$ to the unit sphere $\mathbf{U}$. Each node $\mathbf{P} = (x, y, z) \in \mathbf{M}$ mapped to the spherical position $\mathbf{u} = S(\mathbf{P})$ is represented by the spherical coordinates $\mathbf{u} = (\sin\theta\cos\varphi, \sin\theta\sin\varphi, \cos\theta)$ where $\theta \in [0, \pi]$ and $\varphi \in [0, 2\pi)$ are the polar and azimuth angles, respectively. The SH
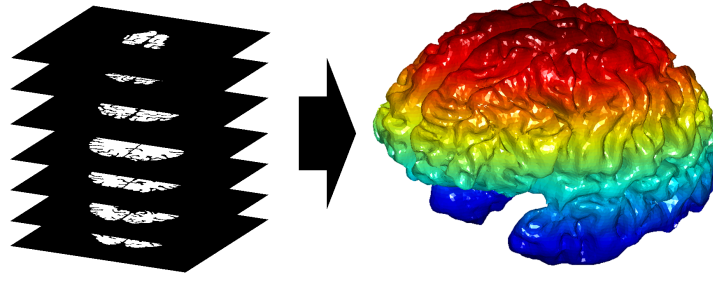
Fig. 4. Illustrating the process of generating a high-resolution 3D mesh for the brain surface from a stack of successive segmented 2D T1-weighted MR image slices.

$Y_{\alpha\beta}$ of degree α and order β is defined as [19]:

$$Y_{\alpha\beta} = \begin{cases} c_{\alpha\beta} G_\alpha^{|\beta|} \cos\theta \sin(|\beta|\varphi) & -\alpha \leq \beta \leq -1 \\ \frac{c_{\alpha\beta}}{\sqrt{2}} G_\alpha^{|\beta|} \cos\theta & \beta = 0 \\ c_{\alpha\beta} G_\alpha^{|\beta|} \cos\theta \cos(|\beta|\varphi) & 1 \leq \beta \leq \alpha \end{cases} \qquad (4)$$

where $c_{\alpha\beta} = \left(\frac{2\alpha+1}{2\pi} \frac{(\alpha-|\beta|)!}{(\alpha+|\beta|)!} \right)^{\frac{1}{2}}$ and $G_\alpha^{|\beta|}$ is the associated Legendre polynomial of degree α and order β. For the fixed α, the polynomials G_α^β are orthogonal over the range $[-1, 1]$. As shown in [19], the Legendre polynomials are an effective means of calculating SHs, and this is the main motivation behind their use in this work.

The brain can be simply reconstructed from the SPHARMs of Eq. (4). In the case of a SPHARM expansion, the standard least-square fitting does suffers from some inaccuracy with the complexity of the 3D shape of the brain, and may inadvertently alter some information that can be used to discriminate between AD, MCI, and control individuals. To address this problem, we utilize an iterative residual fitting by Shen et al. [20] that improves the approximations of the 3D gyrifications on the brain.

3.1   Quantitative brain shape analysis

To perform a quantitative analysis of the brain shape we propose two techniques for measuring the complexity of the cerebral cortex: SPHARM reconstruction error and surface complexity.

SPHARM reconstruction error: Due to the unit sphere mapping, the original brain mesh for each subject is inherently aligned with the mesh that is the SPHARM approximation. As the brain is reconstructed using the methods proposed in Section 3 we can measure the error (using Euclidean distance) between the original brain mesh nodes and the SPHARM approximated brain mesh nodes. This error generates a reconstruction error curve that is unique to each subject. Unlike our previous work [17] that narrowly examined the first few

interactions between individual reconstructions, we propose that examining the area under each of these curves will serve as a more robust metric for the brain.
Surface complexity: We also propose a new metric for examining the complexity of the brain using the SPHARM coefficients. For a unit sphere f, having a SPHARM expansion as shown in Eq. (4), we compute the surface complexity metric. $S(f)$ is defined as:

$$
\begin{aligned}
S(f) &= \sum_{N=0}^{\infty} \varepsilon_N^2 \\
&= \sum_{N=0}^{\infty} N B_N^2
\end{aligned}
\tag{5}
$$

where N is the number of harmonics, and b are the previously calculated SPHARM coefficients. The squared residual ε_N^2 is defined as:

$$
\begin{aligned}
\varepsilon_N^2 &= \|f - f_N\|^2 \\
&= \|\sum_{n=N+1}^{\infty} \sum_{m=-n}^{n} b_{nm} Y_n^m\|^2 \\
&= \sum_{n=N+1}^{\infty} \sum_{m=-n}^{n} |b_{nm}|^2 \\
&= \sum_{n=N+1}^{\infty} B_n^2
\end{aligned}
\tag{6}
$$

For use in 3D SPHARM analysis there are three sets of coefficients for each direction, x, y and z. Therefore the surface complexity is expanded from Eq. 6 to be defined as:

$$
S(f) = \frac{\sum_{N=0}^{\infty} N(B_{N,x}^2 + B_{N,y}^2 + B_{N,z}^2)}{\|f_x\|^2 + \|f_y\|^2 + \|f_z\|^2}
\tag{7}
$$

This metric generates a unique curve for each subject similar to the SPHARM reconstruction error curves. Some of the advantages to this calculation are that it relies solely on the coefficients, making it a self contained metric, and it serves to represent the average degree of SPHARM expansion. It is also a convergent metric, and can be computed over the range of harmonics of interest. The surface complexity is a second unique metric for examining the cerebral cortex.

Based on previous studies [21–23] of the gyral index, we hypothesize that the complexity of the brain for control subjects are lower than MCI and AD subjects, with AD being the highest complexity. In terms of SPHARM, this means that less spherical harmonics are requires to accurately approximate the brain gyrifications. We therefore hypothesize that the overall area under the SPHARM reconstruction error curve and the surface complexity curve will be lower for control individuals. We propose the novel use of the SPHARM reconstruction error and surface complexity curves to identify AD, MCI and control subjects.

Our framework has been evaluated on 384 subjects, 30 of which were provided to us by the CADDementia challenge organizers for training, and the other 354 subjects were used for testing. The test data were collected from multicenter clinical-representative T1-weighted MRI data of patients with Alzheimer's disease (AD), mild cognitive impairment (MCI) and healthy controls. To distinguish between the AD, MCI, and control subjects, we used a K-nearest neighbor classifier learning statistical characteristics of the extracted indexes. To build the classifier, we used 8% of the data sets for training for testing.

References

1. Alzheimers Association: 2014 Alzheimer's disease facts and figures. Alzheimer's & Dementia **10**(2) (2014) 47–92
2. Balafar, M.A., Ramli, A.R., Saripan, M.I., Mashohor, S.: Review of brain mri image segmentation methods. Artificial Intelligence Review **33**(3) (2010) 261–274
3. Viola, P., Wells III, W.M.: Alignment by maximization of mutual information. International Journal of Computer Vision **24**(2) (1997) 137–154
4. Zhang, Y., et al.: Segmentation of brain mr images through a hidden markov random field model and the expectation-maximization algorithm. Medical Imaging, IEEE Transactions on **20**(1) (2001) 45–57
5. Farag, A., El-Baz, A., Gimel'farb, G.: Precise segmentation of multimodal images. IEEE Transactions on Image Processing **15**(4) (2006) 952–968
6. Gimel'farb, G.L., Farag, A.A., El-Baz, A.: Expectation-maximization for a linear combination of gaussians. In: Proceedings of IEEE International Conference on Pattern Recognition, (ICPR'04), Cambridge, UK, August 23–26 (2004) 422–425
7. Farag, A., El-Baz, A., Gimel'farb, G.: Density estimation using modified expectation maximization for a linear combination of Gaussians. In: Proceedings of IEEE International Conference on Image Processing, (ICIP'04). Volume 3., Singapore, October 24-27 (2004) 1871–1874
8. El-Baz, A., Gimel'farb, G.: EM–based approximation of empirical distributions with linear combinations of discrete Gaussians. In: Proceedings of IEEE International Conference on Image Processing, (ICIP'07), San Antonio, Texas, USA, September 16–19 (2007)
9. El-Baz, A., Elnakib, A., Khalifa, F., El-Ghar, M.A., McClure, P., Soliman, A., Gimel'farb, G.: Precise segmentation of 3-D magnetic resonance angiography. IEEE Transactions on Biomedical Engineering **59**(7) (2012) 2019–2029
10. Webb, A.R.: Statistical pattern recognition. John Wiley & Sons (2003)
11. Wilson, D., Noble, J.A.: An adaptive segmentation algorithm for time-of-flight MRA data. IEEE Transactions on Medical Imaging **18**(10) (1999) 938–945
12. El-Baz, A.: Novel stochastic models for medical image analysis. PhD thesis, University of Louisville, Louisville, KY, USA (2006)
13. Humphrey, J.D.: Cardiovascular solid mechanics: cells, tissues, and organs. Springer (2002)
14. Alansary, A., Soliman, A., Nitzken, M., Khalifa, F., Elnakib, A., Casanova, M.F., El-Baz, A.: An Integrated Geometrical and Stochastic Approach for Accurate Infant Brain Extraction. In: Proceedings IEEE International Conference on Image Processing, ICIP–2014, Paris, France, October 27–30 (2014) in press
15. Gerig, G., Styner, M., Jones, D., Weinberger, D., Lieberman, J.: Shape analysis of brain ventricles using spharm. In: Mathematical Methods in Biomedical Image Analysis, 2001. MMBIA 2001. IEEE Workshop on, IEEE (2001) 171–178
16. Chung, M.K., Dalton, K.M., Shen, L., Evans, A.C., Davidson, R.J.: Weighted fourier series representation and its application to quantifying the amount of gray matter. Medical Imaging, IEEE Transactions on **26**(4) (2007) 566–581
17. Nitzken, M., Casanova, M., Gimel'farb, G., Khalifa, F., Elnakib, A., Switala, A.E., El-Baz, A.: 3D shape analysis of the brain cortex with application to autism. In: Biomedical Imaging: From Nano to Macro, 2011 IEEE International Symposium on, IEEE (2011) 1847–1850
18. Fang, Q., Boas, D.A.: Tetrahedral mesh generation from volumetric binary and grayscale images. In: Biomedical Imaging: From Nano to Macro, 2009. ISBI'09. IEEE International Symposium on, IEEE (2009) 1142–1145

19. Courant, R., Hilbert, D.: Methods of Mathematical Physics. Volume 1. London: Interscience (1953)
20. Shen, L., Chung, M.K.: Large-scale modeling of parametric surfaces using spherical harmonics. In: 3D Data Processing, Visualization, and Transmission, Third International Symposium on, IEEE (2006) 294–301
21. Casanova, M.F., Araque, J., Giedd, J., Rumsey, J.M.: Reduced brain size and gyrification in the brains of dyslexic patients. Journal of Child Neurology **19**(4) (2004) 275–281
22. Eliez, S., Rumsey, J.M., Giedd, J.N., Schmitt, J.E., Patwardhan, A.J., Reiss, A.L.: Morphological alteration of temporal lobe gray matter in dyslexia: an MRI study. Journal of Child Psychology and Psychiatry **41**(5) (2000) 637–644
23. Silani, G., Frith, U., Demonet, J.F., Fazio, F., Perani, D., Price, C., Frith, C., Paulesu, E.: Brain abnormalities underlying altered activation in dyslexia: a voxel based morphometry study. Brain **128**(10) (2005) 2453–2461